Using the gradient of human cortical bone properties to determine age-related bone changes via ultrasonic guided waves

Cécile Baron[a,*]

[a] *Aix-Marseille Univ, ISM, 13288, Marseille, France*
CNRS, UMR 7287, 13288, Marseille, France

Abstract

Bone fragility depends not only on bone mass but also on bone quality (structure and material). To accurately evaluate fracture risk or propose therapeutic treatment, clinicians need a criterion which reflects the determinants of bone strength: geometry, structure and material. In human long bone, the changes due to aging, accentuated by osteoporosis are often revealed through the trabecularization of cortical bone, i.e. increased porosity of endosteal bone inducing a thinning of the cortex. Consequently, the intra-cortical porosity gradient corresponding to the spatial variation in porosity across the cortical thickness is representative of loss of mass, changes in geometry (thinning) and variations in structure (porosity).

This paper examines the gradient of material properties and its age-related evolution as a relevant parameter to assess bone geometry, structure and material. By applying a homogenization process, cortical bone can be considered as an anisotropic functionally graded material with variations in material

*Corresponding author
Email address: `cecile.baron@univ-amu.fr` (Cécile Baron)

Preprint submitted to Ultrasound in Medicine and Biology *February 1, 2012*

properties. A semi-analytical method based on the sextic Stroh formalism is proposed to solve the wave equation in an anisotropic functionally graded waveguide for two geometries, a plate and a tube, without using a multilayered model to represent the structure. This method provides an analytical solution called the matricant and explicitly expressed under the Peano series expansion form.
Our findings indicate that ultrasonic guided waves are sensitive to the age-related evolution of realistic gradients in human bone properties across the cortical thickness and have their place in a multimodal clinical protocol.
Keywords: cortical bone, porosity gradient, elastic wave propagation, Stroh formalism, waveguide

Introduction

It is now widely accepted that bone strength relies on two main factors: bone density and bone quality. Thus, accurate information is needed on the quantity of bone, the way it is organized and the mechanical quality of its constituent materials (elastic properties) in order to accurately evaluate fracture risk, to optimize treatment (time and dosage) and to reduce adverse effects. Nowadays, bone densitometry as determined by DXA (Dual-energy X-ray Absorptiometry) is the gold standard technique used to diagnose osteoporosis and to decide on treatment. It provides a value for BMD (Bone Mineral Density) which is compared to that of a reference population to assess whether the patient is "normal", presents with osteopenia or presents with osteoporosis.

One of the fundamental challenges in bone characterization is to identify the relevant parameters, which have to be correlated to the pathology and accessible through clinical measurements. Moreover, as with all technological developments for biomedical applications, it is essential to respect certain criteria: techniques should be non-destructive, non-invasive and non-radiating. Quantitative Ultrasound techniques are good candidates on all these conditions. Yet, they continue to struggle for acceptance against the gold standard of DXA analysis, partly because no single physical parameter has been identified to represent the "structure, geometry, material" triangle. For a long time now, it has been recognized that bone mass alone (Bone Mineral Density) is insufficient to predict risk of fracture (Faulkner, 2000; Robbins et al., 2005). It has been reported that BMD alone explains less than half the risk of hip fractures (Marshall et al., 1996). Several studies have revealed cases where the effect of BMD on risk of fracture is atypical. Postmenopausal Chinese women, for example, have significantly lower hip bone mineral density than white women and are classified at higher risk, but in fact they have fewer fractures (Tobias et al., 1994; Xiaoge et al., 2000).

It would appear, then, that bone quantity alone is not sufficient to evaluate bone fragility, and that bone geometry and quality are key factors which significantly affect bone strength (Augat et al., 1996; Ammann and Rizzoli, 2003; Moilanen et al., 2007; Gregory and Aspden, 2008).

Moreover, even though BMD combines cortical and trabecular bone mass, the majority of what is measured by DXA is trabecular bone. As a consequence, osteoporosis treatments focus primarily on trabecular bone. Yet while both bone compartments contribute to bone strength (Manske et al., 2009), several recent studies point out that cortical bone is a critical component in determining fracture resistance at the femoral neck (Augat and Schorlemmer, 2006; Holzer et al., 2009; Treece et al., 2010).

At the same time, as imaging techniques become more and more accurate, a newly visible characteristic of bone is emerging: intracortical porosity changes gradually across the thickness of long bones (Bousson et al., 2001; Tatarinov et al., 2005; Haïat et al., 2009; Grimal et al., 2011). When homogenization methods are applied to cortical bone, it can be viewed as a functionally graded material at mesoscopic scale.

Among the changes in cortical bone due to aging, there is a joint process accentuated by osteoporosis: trabecularization of the endosteal part leading to thinning of the cortex. Therefore the gradient (spatial variation) of intracortical porosity is a parameter representative of increased variation in porosity across a reduced thickness, and should be relevant to evaluate the combined effect of thinning and trabecularization. This gradient of intracortical porosity induces gradients of material properties (mass density and stiffness coefficients). Thus, characterizing the gradient of the bone properties across the cortical thickness, will provide information on structure (porosity), geometry (thickness) and material (stiffness).

In this study, we consider the diaphysis of long bone, in particular cortical bone. We model cortical bone as a one-phase material with varying mechanical properties (mass density and stiffness coefficients). Modeling how porosity changes across the cortical thickness, and translating this variation in a microscopic property to mesoscopic level, are complex tasks. We base ourselves on two studies (Bousson et al., 2000; Grimal et al., 2011), and define a mesoscopic functionally graded material (FGM) model. A semi-analytical method is proposed to solve the wave equation in an FGM waveguide. This method, based on the Stroh formalism, allows us to avoid a multilayered media approximation and to consider a cylindrical geometry in association with an anisotropic material. According to numerous experimental studies (Reilly and Burnstein, 1974; Dong and Guo, 2004; Lakshmanan et al., 2007), human cortical bone is assumed to be a transversely isotropic material. Here cortical bone is represented by a transversely isotropic plate or tube in vacuum. The dispersion curves of the guided waves are explored to evaluate the sensitivity of these waves to a realistic variation in intracortical porosity.

Materials and Methods

Cortical bone as an anisotropic Functionally Graded Material waveguide

The model takes into account the anisotropy and the heterogeneity of cortical bone: it is considered as transversely isotropic with linearly varying material properties. Moreover, two geometries are investigated for long bone modeled as a plate or as a tube with realistic dimensions.

Functionally Graded Material properties

Here, every attempt was made to model realistic variation in porosity across the cortical thickness. Based on previous work reported on femoral cortical bone samples from skeletons (Bousson et al., 2000, 2001), we focus on a solely female population (86 subjects) aged from 11 to 96. We use these authors' 3-point measurement of porosity (periosteal, mid-cortical and endosteal regions) to infer the evolution of porosity across the cortical thickness.

Then, the evolution of intracortical porosity (microscopic scale) is translated into a variation in the elastic properties of the bone at the mesoscopic level by using the regression models (size of the mesodomain $L = 0.5$ mm) proposed by Grimal and colleagues (Grimal et al., 2011). Thereby, the Young's and shear moduli and the Poisson ratios are expressed as a function of porosity.

Porosity varies with position across the thickness of the bone, and consequently the Young's and shear moduli and Poisson ratios are also dependent on the spatial variable across the thickness (x-variable for the plate and r-variable for the tube), except for ν_{TL}, which is assumed to be constant at

0.3.

Then we deduce the five independent stiffness coefficients as five spatially-dependent functions from the following equations:

$$\begin{gathered} c_{11}=\frac{E_T(1-\nu_{TL}\nu_{LT})}{\Delta};\ c_{12}=\frac{E_T(\nu_{TT}+\nu_{TL}\nu_{LT})}{\Delta}; \\ c_{13}=\frac{E_T(\nu_{LT}+\nu_{TT}\nu_{LT})}{\Delta};\ c_{33}=\frac{E_L(1-\nu_{TT}\nu_{TT})}{\Delta}; \\ c_{44}=G_{LT}; \end{gathered} \tag{1}$$

with $\Delta=\nu_{TT}^2+2\nu_{LT}\nu_{TL}+2\nu_{LT}\nu_{TL}\nu_{TT}$.

Note the correspondence $1\rightarrow T; 2\rightarrow T; 3\rightarrow L$ where L and T are *longitudinal* and *transverse* respectively .

The degree of porosity (from 0 to 30%) does not disturb the crystallographic symmetry of the material at the mesoscopic scale (Baron et al., 2007): the thermodynamic conditions are still valid.

Figure 1 shows that the stiffness coefficients can be supposed to linearly vary according to porosity across the cortical thickness for each age group. A linear regression provides an affine function representing the evolution of the stiffness coefficients across the cortical thickness.Thus, the elastic properties vary from a maximum value in the periosteal region to a minimum value in the endosteal region (Table 1).

A classical mixture law is used to obtain mass density as a function of spatial variable ξ, where $\xi=x$ for the plate and $\xi=r$ for the tube. We assume that the pores are filled with water considered as a perfect fluid:

$$\rho(\xi)=\rho_{bone}(1-p(\xi))+\rho_{water}p(\xi); \tag{2}$$

with p the porosity, $\rho_{bone}=1.9$ g/cm^3 and $\rho_{water}=1$ g/cm^3.

Choice of waveguide geometry

It was essential to set realistic parameters for the geometry of the model. For a first approximation, long bone can be modeled as a plate, ignoring the curvature effect on guided wave propagation (Lefebvre et al., 2002; Bossy et al., 2004; Protopappas et al., 2006; Baron, 2011). However, a more realistic shape for long bone is a tube (Protopappas et al., 2007), and here both geometries were investigated. For the plate, the set of parameters was reduced to the thickness, taken as decreasing with age (Bousson et al., 2001)(Table 2). For the tube, one of the parameters known to influence guided wave propagation is the ratio of thickness over outer radius (Nishino et al., 2001; Baron, 2011). Here too, thickness was taken from (Bousson et al., 2001). Previous findings (Carter et al., 1996; Feik et al., 2005) have established that the outer diameter remains the same after 30 years; in this study, it is fixed at 24 mm and the thinning of the cortical wall with age is represented by an increase in the inner diameter to reach the thickness measured by Bousson and colleagues (Bousson et al., 2001).

Ultrasonic guided waves

We consider an elastic waveguide (plate or tube) of thickness t placed in vacuum. The coordinate systems (x, y, z) for the plate and (r, θ, z) for the tube are defined with the z-axis corresponding to the axis of the long bone and x and r representing the spatial variables along the cortical thickness.

The variable x describes the thickness of the plate from 0 to t. The radius of the tube r varies from a_0 to a_q, respectively the inner and outer radius of the tube (Figure 2).In order to simplify the notation we use the variable ξ where $\xi = x, r$.

The elastic waveguide is considered to be anisotropic and is liable to present continuously varying properties across its thickness ($\mathbf{e}_x$-axis or $\mathbf{e}_r$-axis). These mechanical properties are represented by the stiffness tensor $\mathbb{C} = \mathbb{C}(\xi)$ and the mass density $\rho = \rho(\xi)$.

System equations

The momentum conservation equation associated with the constitutive law of linear elasticity (Hooke's law) gives the following equations:

$$\begin{cases} \mathrm{div}\boldsymbol{\sigma} = \rho \dfrac{\partial^2 \mathbf{u}}{\partial t^2}, \\ \boldsymbol{\sigma} = \dfrac{1}{2}\mathbb{C}\left(\mathrm{grad}\mathbf{u} + \mathrm{grad}^T\mathbf{u}\right), \end{cases} \tag{3}$$

where $\mathbf{u}$ is the displacement vector and $\boldsymbol{\sigma}$ the stress tensor.

- for the plate

  We assume that the structure is two-dimensional and that the guided waves travel in the plane $y = 0$; in the following, this coordinate is implicit and is omitted in the mathematical expressions. Solutions are sought for the vectors of displacement ($\mathbf{u}$) and traction ($\boldsymbol{\sigma}_x = \boldsymbol{\sigma}.\mathbf{e}_x$) expressed in the cartesian coordinates (x, z) with the basis $\{\mathbf{e}_x, \mathbf{e}_z\}$:

$$\begin{aligned} \mathbf{u}(x, z; t) &= \mathbf{U}(x) \exp \imath \left(k_z z - \omega t\right), \\ \boldsymbol{\sigma}_x(x, z; t) &= \mathbf{T}(x) \exp \imath \left(k_z z - \omega t\right); \end{aligned} \tag{4}$$

  with k_z the axial wavenumber. The modes propagating in such a structure are called Lamb modes. We distinguish two types of Lamb modes: symmetrical (S-modes) and anti-symmetrical branches (A-modes) (Lamb, 1917).

- for the tube

  We seek to solve the wave equation for displacement vector ($\mathbf{u}$) and radial traction vector ($\boldsymbol{\sigma}_r = \boldsymbol{\sigma}.\mathbf{e}_r$) expressed in the cylindrical coordinates (r, θ, z) with the basis $\{\mathbf{e}_r, \mathbf{e}_\theta, \mathbf{e}_z\}$:

$$\begin{aligned} \mathbf{u}(r, \theta, z; t) &= \mathbf{U}^{(n)}(r) \exp \imath \left(n\theta + k_z z - \omega t\right), \\ \boldsymbol{\sigma}_r(r, \theta, z; t) &= \mathbf{T}^{(n)}(r) \exp \imath \left(n\theta + k_z z - \omega t\right); \end{aligned} \tag{5}$$

  with k_z the axial wavenumber and n the circumferential wavenumber. We distinguish two types of waves propagating in a cylindrical waveguide: *circumferential waves* and *axial waves*. *Circumferential waves* are waves traveling in planes perpendicular to the axis direction. They correspond to $u_z(r) = 0\,(\forall r)$, $k_z = 0$ and $n = k_\theta a_q$. *Axial waves* are waves traveling along the axis direction, the circumferential wavenumber is an integer $n = 0, 1, 2, ...$ Among the *axial waves*, we distinguish three types of modes numbered with two parameters (n, m) representing the circumferential wavenumber and the order of the branches: longitudinal (L), flexural (F) and torsional (T) modes. The longitudinal and torsional modes are axially symmetric $(n = 0)$ and denoted $L(0, m)$ and $T(0, m)$. The flexural modes are non-axially symmetric $(n \geq 1)$ and are denoted $F(n, m)$ (Gazis, 1959). In this paper, we focus on longitudinal and first flexural modes $(n = 1)$.

A closed-form solution: the matricant

Introducing the expression (4 or 5) into the equation (3), we obtain the wave equation in the form of a second-order differential equation with non-constant coefficients. In the general case, there is no analytical solution to the problem thus formulated. Most current methods of solving the wave equation in unidirectionally heterogeneous media are derived from the Thomson-Haskell method (Thomson, 1950; Haskell, 1953). These methods are appropriate for multilayered structures (Kenneth, 1982; Lévesque and Piché, 1992; Wang and Rokhlin, 2001; Hosten and Castaings, 2003). However, for continuously varying media, these techniques replace the continuous profiles of properties by step-wise functions, thereby making the problem approximate, even before the resolution step. The accuracy of the solution, like its validity domain, are thus hard to evaluate. Moreover, a multilayered model of functionally graded waveguides creates "virtual" interfaces likely to induce artefacts. Lastly, for generally anisotropic cylinders, the solutions cannot be expressed analytically, even for homogeneous layers (Mirsky, 1964; Nelson et al., 1971; Soldatos and Jianqiao, 1994).

To solve the exact problem, that is, to maintain the continuity of the variation in properties , and to take into account the anisotropy of cylindrical waveguides, we write the wave equation under the sextic Stroh formalism (Stroh, 1962) in the form of an ordinary differential equations system with non-constant coefficients for which an analytical solution exists: the matricant (Pease, 1965; Baron, 2005).

Hamiltonian form of the wave equation. In the Fourier domain, the wave equation can be written as:

- for the plate

$$\frac{d}{dx}\boldsymbol{\eta}(x) = \mathbf{Q}(x)\boldsymbol{\eta}(x); \tag{6}$$

- for the tube

$$\frac{d}{dr}\boldsymbol{\eta}(r) = \frac{1}{r}\mathbf{Q}(r)\boldsymbol{\eta}(r). \tag{7}$$

The components of the state-vector $\boldsymbol{\eta}(\xi)$ are the components of the displacement vector $\mathbf{u}$ and the components of the traction vector $\boldsymbol{\sigma}_\xi$. As for the matrix $\mathbf{Q}(\xi)$, it contains all the information about heterogeneity: it is expressed from the stiffness coefficients of the waveguide in the appropriate system of coordinates (cartesian for the plate and cylindrical for the tube) and from two acoustical parameters (wavenumbers, angular frequency, horizontal slowness). Detailed expressions of $\mathbf{Q}(\xi)$ are given in appendix a for the case of a material with hexagonal crystallographic symmetry; but it can be expressed for any type of anisotropy (Shuvalov, 2003).

Explicit solution: the Peano expansion of the matricant. The wave equation thus formulated has an analytical solution expressed between a reference point ξ_0 and some point along the cortical thickness direction ξ. This solution is called the matricant and is explicitly written in the form of the Peano series expansion:

$$\mathbf{M}(\xi, \xi_0) = \mathbf{I} + \int_{\xi_0}^{\xi} \mathbf{Q}(\varsigma)d\varsigma + \int_{\xi_0}^{\xi} \mathbf{Q}(\varsigma) \int_{\xi_0}^{\varsigma} \mathbf{Q}(\varsigma_1)d\varsigma_1 d\varsigma + ..., \tag{8}$$

where $\mathbf{I}$ is the identity matrix of dimension $(6, 6)$. If the matrix $\mathbf{Q}(\xi)$ is bounded in the study interval, these series are always convergent (Baron, 2005). The components of the matrix $\mathbf{Q}$ are continuous in ξ and the study interval is bounded (thickness of the waveguide), consequently the hypothesis is always borne out. The matricant verifies the propagator property (Baron, 2005):

$$\boldsymbol{\eta}(\xi) = \mathbf{M}(\xi, \xi_0)\boldsymbol{\eta}(\xi_0). \tag{9}$$

Free boundary conditions. The waveguide is considered to be in vacuum, so the traction vector $\boldsymbol{\sigma}_\xi$ defined in (4 and 5) is null at both interfaces. Using the propagator property of the matricant through the thickness of the structure, equation (9) is written as $\boldsymbol{\eta}(\xi_0 + t) = \mathbf{M}(\xi_0 + t, \xi_0)\boldsymbol{\eta}(\xi_0)$ with $\xi_0 = 0$ for the plate and $\xi_0 = a_0$ for the tube. Factorizing the matricant $\mathbf{M}(\xi_0 + t, \xi_0)$ under four block matrices of dimension $(3, 3)$, equation 9 becomes:

$$\begin{pmatrix} \mathbf{u}(\xi = \xi_0 + t) \\ \mathbf{0} \end{pmatrix} = \begin{pmatrix} \mathbf{M}_1 & \mathbf{M}_2 \\ \mathbf{M}_3 & \mathbf{M}_4 \end{pmatrix} \begin{pmatrix} \mathbf{u}(\xi = \xi_0) \\ \mathbf{0} \end{pmatrix}. \tag{10}$$

Equation (10) has non-trivial solutions for $\det\mathbf{M}_3 = 0$. As detailed in appendix a for a transversely isotropic material and from equation (8), the components of $\mathbf{M}_3$ are bivariate polynomials in (s_z, ω) or (k_z, ω). Consequently, seeking the zeros of $\det\mathbf{M}_3$ amounts to seeking the pairs of values (s_z, ω) or (k_z, ω) which describe the dispersion curves of guided waves propagating in a plate or a tube respectively.

Results

Gradient of porosity

The variation in porosity across the cortical thickness and its age-related evolution are presented in Table 2. Figure 3 shows that a linear profile is a good approximation to model porosity changes. For every age range, $p\% = a\xi + b$, where ξ is the spatial variable along the cortical thickness, $(a, b) \in \Re^2$.

The porosity gradient (%/mm) is deduced from an estimation of the slope a for each age class (Table 2).

Figure 3 clearly shows that porosity sharply increases with age in the endosteal region, whereas it remains fairly stable in the periosteal region. Moreover, cortical thickness greatly decreases with age, from adulthood to old age. These two processes identified by Bousson (Bousson et al., 2000, 2001), are linked under the name trabecularization of the endosteal region.

The age-related evolution of the porosity gradient represented on figure 4 reveals an inverse trend compared to the evolution of BMD (Melton III et al., 2000): it remains almost constant up to the 4th decade and then it increases with advancing age. The regression is exponential, similar to the evolution of the risk of fracture with age reported in the literature (Hui et al., 1988; De Laet et al., 1997; Kanis et al., 2008).

Sensitivity of guided waves to the gradient of material properties

The effect of a realistic intracortical porosity gradient on guided wave propagation was investigated to determine how sensitive the guided waves are to the age-related evolution of long bone strength; in particular, whether they are sensitive both to thinning of the cortex and to increased endosteal porosity during aging. We compared the ultrasonic guided waves' interaction with three planar waveguides and three tubular waveguides modeling the diaphysis of the femur at three different age ranges: [30-39], [60-69] and [80-99] (Bousson et al., 2001). Waveguides dimensions are reported in Table 3. The dispersion curves are plotted as functions of the frequency-thickness product in the usual range for the study of ultrasonic waves in long bones (Bossy et al., 2004; Muller et al., 2005; Tatarinov et al., 2005; Protopappas et al., 2006). For guided waves in long bones, the typical frequency range is between 50 kHz to 350 MHz (Moilanen et al., 2008) to generate wavelengths greater than the cortical thickness (Bossy et al., 2004). Consequently, the frequency-thickness product to be considered is roughly [0.2, 1.5] MHz.mm for [30-39], [0.15, 1.1] MHz.mm for [60-69] and [0.125, 0.875] MHz.mm for [80-99].

The dispersion curves of Lamb modes propagating in plates show measurable differences throughout aging (Figure 5). The discrepancy between the dispersion spectra obtained for each age range grows with the frequency-thickness product. For example, at 1 MHz.mm, the phase velocity of the S_0 mode for the [80-99] age group is 6% lower than for the [30-39] age group, the phase velocity of the A_2 mode for the [60-69] age group is 5% higher than for the [80-99] age group and 10% lower than for the [30-39] age group. All these differences correspond to several thousand meters per second, which are experimentally measurable quantities.

The same trends can be seen from the dispersion curves of the longitudinal and flexural modes propagating in the tubes (Figure 6). The cut-off frequencies of all the modes are distinct for the three age ranges considered (Table 4). The phase velocities are also significantly different: for instance, the discrepancy between the $F(1,3)$-mode phase velocity for [80-99] and the $F(1,3)$-mode phase velocity for [30-39] is about 420 m/s.

One of the critical parameters of long bone strength is cortical thickness. To evaluate cortical thickness, Moilanen and his team showed the relevance of considering the $F(1,1)$ mode instead of the A_0 mode (Moilanen et al., 2007). This is confirmed by our results on the group velocity of these two modes calculated for the three age ranges (Figure 7).

It is clearly shown that around the frequency of 200 kHz used by Moilanen and colleagues, the group velocity of A_0 mode is consistently different from the group velocity of the $F(1,1)$ mode and it appears that the group velocity of the $F(1,1)$ mode is very sensitive to the porosity gradient in the frequency range considered.

Discussion

The Stroh formalism used in this study has several advantages. First, it allows ultrasound propagation to be investigated in a continuously varying medium (FGM) instead of approximating it by a multilayered medium, thus avoiding potential round-off errors and artefacts which cannot be estimated. It provides an exact solution to the exact problem, and the degree of round-off error is manageable (Baron, 2005). Furthermore, this formalism is numerically stable and is applicable to planar and tubular geometries whatever the degree of anisotropy of the material. The conventional methods used to solve the wave equation are unable to deal with cylindrical coordinates coupled with general anisotropy. The Stroh formalism is one of the only ways to provide an analytical solution (Peano expansion of the matricant) to the wave equation in a cylindrical structure whatever the anisotropy of the material (Shuvalov, 2003). Moreover, fluid-loading of the waveguide here can be treated as in the case of the plate (Baron and Naili, 2010). The advantages of this formalism in the context of bone characterization are clear, since long bone can be realistically modeled as an FGM orthotropic tube surrounded by blood and full of marrow. In addition, because this method takes into account actual variations in material properties of long bones, it could prove useful as a reference to validate models which do not allow for the gradient of material properties, confirming the range of validity (frequency domain, thickness range, order of the modes) of the results yielded by such simplified models.

Bone fragility has long been known to be related to the quantity of material (bone density), its quality (stiffness) and its organization (geometry and micro-architecture). A accurate evaluation of fracture risk has to assess these three parameters together. As cortical bone ages, endosteal trabecularization induces thinning of the cortex. Thus, the spatial variation in porosity across the cortical thickness revealed during aging can be taken as the "‘missing"’ parameter to represent bone quality. This is confirmed by figure 4, which illustrates an evolution in porosity gradient with age similar to the evolution in risk of fracture reported in the literature for the vertebra (Cooper et al., 1992) and for the hip (De Laet et al., 1997). As previously pointed out, the gradient of material properties (density and stiffness coefficients) reflects the spatial distribution of the quantity and quality of bone across the cortical thickness. Looking at the dispersion curves obtained here for the plate and for the tube, this discrepancy between the different age ranges appears to be experimentally measurable. Thus, this study indicates that the gradient of homogenized material properties can be evaluated from measured ultrasound velocities.

Solving the inverse problem, however, will be tricky, and further work will be required before this can be achieved. An accurate evaluation of the various factors influencing bone strength would require a wider range of measurements (other ultrasound frequencies, other imaging modalities).

Our work demonstrates the sensitivity of guided waves to realistic variations in the intrinsic properties of human cortical bone: porosity, density, stiffness, as revealed by the gradient in material properties. Nevertheless, it remains difficult to establish a reliable criterion to apply in a clinical protocol. Careful consideration needs to be given to choosing appropriate anatomical sites for ultrasonic evaluation. To avoid too much ultrasound absorption, the most suitable sites are the phalanx, the radius and the tibia (Njeh et al., 2001). These sites are long bones for which the question of the influence of the curvature on wave propagation needs to be addressed (Baron, 2011). The choice of geometric model - plate or tube - is particularly important in pediatrics, since the thickness over outer radius ratio (t/a_q) of growing bone is greater than 0.5. Thus, ultrasound evaluation is a promising alternative technique in pediatrics.

Our model could usefully be extended. Several realistic characteristics can easily be added to the formalism we use. Firstly, how soft tissue affects wave propagation can be modeled by fluid-loading, as examined in a recent paper (Baron and Naili, 2010). Secondly, the gradual variation in the intrinsic properties of the bone matrix described in (Lakshmanan et al., 2007) can be included in the homogenization step and would contribute to the mesoscopic gradient of bone properties.

Furthermore it would be relevant to consider not only the variation in "global" intracortical porosity (the ratio of the volume of pores over the total volume) but also the distribution of pore sizes and of the number of pores across the cortical thickness. In (Bousson et al., 2001), it was noted that increased endosteal porosity arises from an increase in the size of pores rather than from an increase in the number of pores; this difference in the organization of the microstructure may affect the mechanical behavior of the bone.

Conclusion

The gradient of material properties appears here to be relevant to evaluating age-related changes in cortical bone, particularly in the context of osteoporosis and therapeutic follow-up. This paper describes an original method applied to bone characterization able to take into account the heterogeneity (porosity gradient) and the anisotropy (orthotropy) of the material as well as the tubular geometry of the structure, even under *in-vivo* conditions (soft tissue).

Ultrasound evaluation appears a good candidate to characterize long bone (structure, geometry and material); however, the potential of *in-vivo* techniques that take into account the influence of soft tissue and marrow needs to be further explored.

The results we obtain are promising, but the method should be extended, in particular with a view to solving the inverse problem. An *in-vitro* experimental program would validate the feasibility of the ultrasound measurements on bone samples of different ages. It could also evaluate the relevance of using an *in-vivo* characterization of the gradient of properties across the cortical thickness to determine bone strength and the risk of fracture.

Appendix A

$$\frac{d}{dx}\boldsymbol{\eta}(x) = \imath\omega\mathbf{Q}(x)\boldsymbol{\eta}(x), \tag{.1}$$

Plate/tube

Formalism for plate

$$\frac{d}{dx}\begin{pmatrix} \imath\omega\hat{u}_x \\ \imath\omega\hat{u}_z \\ \hat{\sigma}_{xx} \\ \hat{\sigma}_{xz} \end{pmatrix} = \imath\omega \begin{pmatrix} 0 & -c_{13}(x)/c_{11}(x)s_z & 1/c_{11}(x) & 0 \\ s_3 & 0 & 0 & 1/c_{55}(x) \\ \rho(x) & 0 & 0 & -s_z \\ 0 & \rho(x1) - s_z^2\zeta(x) & -c_{13}(x)/c_{11}(x)s_z & 0 \end{pmatrix} \begin{pmatrix} \imath\omega\hat{u}_x \\ \imath\omega\hat{u}_z \\ \hat{\sigma}_{xx} \\ \hat{\sigma}_{xz} \end{pmatrix}, \tag{.2}$$

with the relations :

$$\zeta(x) = c_{33}(x) - \frac{c_{13}^2(x)}{c_{11}(x)}, \quad k_z = \omega s_z, \tag{.3}$$

where s_z is the $\mathbf{z}$-component of the slowness.

Formalism for tube

Expression of the vector $\boldsymbol{\eta}(r)$ and of the matrix $\mathbf{Q}(r)$ for a material with hexagonal crystallographic symmetry (5 independent stiffness coefficients). The symbol $\hat{.}$ represents the quantities in the Fourier domain.

$$\boldsymbol{\eta}(r) = \begin{pmatrix} \hat{u}_r(r), & \hat{u}_\theta(r), & \hat{u}_z(r), & \imath r\hat{\sigma}_{rr}(r), & \imath r\hat{\sigma}_{r\theta}(r), & \imath r\hat{\sigma}_{rz}(r) \end{pmatrix}^T,$$

and

$$
\mathbf{Q}(r) = \frac{1}{r} \left(\begin{array}{cc}
-\frac{c_{12}}{c_{11}} & -\imath n \frac{c_{12}}{c_{11}} \\
-\imath n & 1 \\
-\imath k_z r & 0 \\
\imath \left(\gamma_{12} - r^2 \rho \omega^2\right) & -n\gamma_{12} \\
n\gamma_{12} & \imath n^2 \gamma_{12} + \imath r^2 \left(k_z^2 c_{44} - \rho\omega^2\right) \\
k_z r \gamma_{23} & \imath n k_z r \left(\gamma_{23} + c_{44}\right)
\end{array} \right. \ldots
$$

$$
\ldots \left. \begin{array}{cccc}
-\imath k_z r \frac{c_{13}}{c_{11}} & -\frac{\imath}{c_{11}} & 0 & 0 \\
0 & 0 & -\frac{\imath}{c_{66}} & 0 \\
0 & 0 & 0 & \frac{\imath}{c_{44}} \\
-k_z r \gamma_{23} & \frac{c_{12}}{c_{11}} & -\imath n & -\imath k_z r \\
\imath n k_z r \left(\gamma_{123} + c_{44}\right) & -\imath n \frac{c_{12}}{c_{11}} & -1 & 0 \\
\imath n^2 c_{44} + \imath r^2 \left(k_z^2 \gamma_{13} - \rho\omega^2\right) & -\imath k_z r \frac{c_{13}}{c_{11}} & 0 & 0
\end{array} \right)
$$

with $c_{66} = (c_{11} - c_{12})/2$ and

$$
\gamma_{12} = c_{11} - \frac{c_{12}^2}{c_{11}} \; ; \; \gamma_{13} = c_{33} - \frac{c_{13}^2}{c_{11}} \; ; \; \gamma_{23} = c_{13} - \frac{c_{12}c_{13}}{c_{11}}.
$$

References

Ammann P, Rizzoli R. Bone strength and its determinants. Osteoporos. Int., 2003;14Suppl. 3:S13–S18.

Augat P, Reeb H, Claes LE. Prediction of fracture load at different skeletal sites by geometric properties of the cortical shell. Journal of Bone and Mineral Research, 1996;11:1356–1363.

Augat P, Schorlemmer S. The role of cortical bone and its microstructure in bone strength. Age and ageing, 2006;35suppl 2:ii27–ii31.

Baron C. Le développement en série de Peano du matricant pour l'étude de la propagation d'ondes en milieux continûment variables - Peano expansion of the matricant to study elastic wave propagation in continuously heterogeneous media. Ph.D. thesis, Université Bordeaux 1, France, 2005.

Baron C. Propagation of elastic waves in an anisotropic functionally graded hollow cylinder in vacuum. Ultrasonics, 2011;51:123–130.

Baron C, Naili S. Propagation of elastic waves in a fluid-loaded anisotropic functionally graded waveguide: Application to ultrasound characterization. Journal of Acoustical Society of America, 2010;127:1307–1317.

Baron C, Talmant M, Laugier P. Effect of porosity on effective diagonal stiffness coefficients (c_{ii}) and anisotropy of cortical at 1 MHz: A finite-difference time domain study. Journal of Acoustical Society of America, 2007;122:1810–1817.

Bossy E, Talmant M, Laugier P. Three-dimensional simulations of ultrasonic axial transmission velocity measurement on cortical models. Journal of Acoustical Society of America, 2004;115:2314–2324.

Bousson V, Bergot C, Meunier A, Parlier-Cuau C, Laval-Jeantet AM, Laredo JD. CT of the Middiaphyseal Femur: Cortical Bone Mineral Density end Relation to Porosity. Radiology, 2000;217:179–187.

Bousson V, Meunier A, Bergot C, Vicaut E, Rocha MA, Morais MH, Laval-Jeantet AM, Laredo JD. Distribution of intracortical porosity in human midfemoral cortex by age and gender. Journal of Bone and Mineral Reasearch, 2001;16:1308–1317.

Carter DR, Van Der Meulen MCH, Beaupré GS. Mechanical Factors in Bone Growth and Development. Bone, 1996;18:5S–10S.

Cooper C, Atkinson EJ, MichaelO'Fallon W, Melton JL. Incidence of clinically diagnosed vertebral fractures: A population-based study in Rochester, Minnesota, 1985-1989. Journal of Bone and Mineral Research, 1992;87:221Ũ227.

De Laet CE, van Hout BA, Burger H, Hofman A, Pols HA. Bone density and risk of hip fracture in men and women: cross sectional analysis. British Medical Journal, 1997;315:221–225.

Dong XN, Guo XE. The dependence of transversely isotropic elasticity of human femoral cortical bone on porosity. Journal of Biomechanics, 2004;37:1281–1287.

Faulkner KG. Bone matters: Are density increases necessary to reduce fracture risk? Journal of Bone and Mineral Research, 2000;15:183–187.

Feik SA, Thomas DL, Clement JG. Age trends in remodeling of the femoral midshaft differ between the sexes. Journal of Orthopaedic Research, 2005;14:590–597.

Gazis DC. Three-dimensional investigation of the propagation of waves in hollow circular cylinders. I. Analytical foundation. Journal of Acoustical Society of America, 1959;31:568–573.

Gregory JS, Aspden RM. Femoral geometry as a risk factor for osteoporotic hip fracture in men and women. Medical Engineering & Physics, 2008;30:1275Ũ1286.

Grimal G, Raum K, Gerisch A, Laugier P. A determination of the minimum sizes of representative volume elements for the prediction of cortical bone elastic properties. Biomechanics and Modeling in Mechanobiology, 2011;OnLineFirst^{TM}:1–13.

Haïat G, Naili S, Grimal Q, Talmant M. Influence of a gradient of material properties on ultrasonic wave propagation in cortical bone: Application to axial transmission. Journal of Acoustical Society of America, 2009;125:4043–4052.

Haskell NA. The dispersion of surface waves on multilayered media. Bulletin of the Seismological Society of America, 1953;43:377–393.

Holzer G, von Skrbensky G, Holzer LA, Pichl W. Hip fractures and the contribution of cortical versus trabecular bone to femoral neck strength. Journal of Bone and Mineral Research, 2009;243:468–474.

Hosten B, Castaings M. Surface impedance matrices to model the propagation in multilayered media. Ultrasonics, 2003;41:501–507.

Hui SL, Slemenda CW, Johnston CJ. Age and Bone Mass as Predictors of Fracture in a Prospective Study. Journal of Clinical Investigation, 1988;80:1804–1809.

Kanis JA, Johnell O, Oden A, Johansson H, McCloskey A. FRAXŹ and the assessment of fracture probability in men and women from the UK. Osteoporosis International, 2008;19:385Ű397.

Kenneth EG. A propagator matrix method for periodically stratified media. Journal of Acoustical Society of America, 1982;731:137–142.

Lakshmanan S, Bodi A, Raum K. Assessment of anisotropic tissue elasticity of cortical bone from high-resolution, angular acoustic measurements. IEEE Trans Ultrason Ferroelectr Freq Control, 2007;54:1560–1570.

Lamb H. On waves in an elastic plate. Proceedings of the Royal Society of London A., 1917;93:114–128.

Lefebvre F, Deblock Y, Campistron P, Ahite D, Fabre JJ. Development of a new ultrasonic technique for bone and biomaterials in vitro characterization. Journal of Biomedical Material Research, Part B, 2002;63:441–446.

Lévesque D, Piché L. A robust transfer matrix simulation for ultrasonic response of multilayered absorbing media. Journal of Acoustical Society of America, 1992;92:452–467.

Manske SL, Liu-Ambrose T, Cooper DML, Kontulainen S, Guy P, Forster BB, McKay HA. Cortical and trabecular bone in the femoral neck both contribute to proximal femur failure load prediction. Osteoporosis International, 2009;203:445–453.

Marshall D, Johnell O, Wedel H. Meta-analysis of how well measures of bone mineral density predict occurrence of osteoporotic fractures. British Medical Journal, 1996;312:1254–1259.

Melton III LJ, Khosla S, Atkinson EJ, O'Connor MK, O'Fallon WM, Riggs BL. Cross-sectional versus longitudinal evaluation of bone loss in men and women. Osteoporosis International, 2000;11:592–599.

Mirsky I. Axisymmetric vibrations of orthotropic cylinders. Journal of the Acoustical Society of America, 1964;36:2106–2112.

Moilanen P, Nicholson PHF, Kilappa V, Cheng S, Timonen J. Assessment of the cortical thickness using ultrasonic guided waves: Modeling and *in vitro* study. Ultrasound in Medicine and Biology, 2007;33:254–262.

Moilanen P, Talmant M, Kilappa V, Nicholson PHF, Cheng S, Timonen J, Laugier P. Modeling the impact of soft tissue on axial transmission measurements of ultrasonic guided waves in human radius. Journal of the Acoustical Society of America, 2008;124:2364–2373.

Muller M, Moilanen P, Bossy E, Nicholson PHF, Kilappa V, Timonen J, Talmant M, Cheng S, Laugier P. Comparison of three ultrasonic axial transmission methods for bone assessment. Ultrasound in Medicine and Biology, 2005;31:633–642.

Nelson R, Dong S, Kalkra R. Vibrations and waves in laminated orthotropic circular cylinders. Journal of Sound and Vibration, 1971;18:429–444.

Nishino H, Takashina S, Uchida F, Takemoto M, Ono K. Modal analysis of hollow cylindrical guided waves and applications. Japonese Journal of Applied Physics, 2001;301:364–370.

Njeh C, Saeed I, Grigorian M, Kendler D, Fan B, Shepherd J, McClung M, Drake W, Genant H. Assessment of bone status using speed of sound at multiple sites. Ultrasound in Medicine and Biology, 2001;27:1337–1345.

Pease MC. Methods of Matrix Algebra. Academic Press, New York, 1965.

Protopappas V, Fotiadis D, Malizos K. Guided ultrasound wave propagation in intact and healing long bone. Ultrasound in Medicine and Biology, 2006;32:693–708.

Protopappas V, Kourtis IC, Kourtis LC, Malizos K, Massalas CV, Fotiadis D. Three-dimensional finite element modeling of guided ultrasound wave propagation in intact and healing long bones. Journal of the Acoustical Society of America, 2007;121:3907–3921.

Reilly DT, Burnstein AH. The mechanical properties of cortical bone. J. Bone Joint Surg. Am., 1974;56:1001–1022.

Robbins JA, Schott AM, Garnero P, Delmas PD, Hans D, Meunier PJ. Risk factors for hip fracture in women with high BMD: EPIDOS study. Osteoporosis International, 2005;16:149–154.

Shuvalov A. A sextic formalism for three-dimensional elastodynamics of cylindrically anisotropic radially inhomogeneous materials. Proceedings of the Royal Society of London A., 2003;459:1611–1639.

Soldatos K, Jianqiao Y. Wave propagation in anisotropic laminated hollow cylinders of infinite extent. Journal of the Acoustical Society of America, 1994;96:3744–3752.

Stroh AN. Steady state problems in anisotropic elasticity. Journal of Mathematics and Physics, 1962;41:77–103.

Tatarinov A, Sarvazyan N, Sarvazyan A. Use of multiple acoustic wave modes for assessment of long bones: model study. Ultrasonics, 2005;438:672–680.

Thomson WT. Transmission of elastic waves through a stratified solid medium. Journal of Applied Physics, 1950;21:89–93.

Tobias JH, Cook DG, Chambers TJ, Dalzell N. A comparison of bone mineral density between caucasian, Asian and Afro-Caribbean women. Clinical Science, 1994;87:587–591.

Treece G, Gee A, Mayhew P, Poole K. High resolution cortical bone thickness measurement from clinical CT data. Medical Image Analysis, 2010;143:276–290.

Wang L, Rokhlin SI. Stable reformulation of transfer matrix method for wave propagation in layered anisotropic media. Ultrasonics, 2001;39:413–424.

Xiaoge D, Eryuan L, Xianping W, Zhiguang Z, Gan H, Zaijing J, Xiaoli P, Hongzhuan T, Hanwen W. Bone mineral density differences at the femoral neck and Ward's triangle: a comparison study on the reference data between Chinese and caucasian women. Calcified Tissue International, 2000;67:195–198.

Figure Captions

Figure 1: Variation in stiffness coefficients over porosity: $c_{11} = c_{22}\,(\diamond)$, $c_{12}\,(\square)$, $c_{13} = c_{23}\,(\Delta)$, $c_{33}\,(\times)$, $c_{44} = c_{55}\,(*)$, $c_{66}\,(\bullet)$.

Figure 2: Geometrical configuration of the waveguides.

Figure 3: Variation in porosity across the cortical thickness: linear regression for each age range ($R^2 \geq 0.9$).

Figure 4: Age-related evolution of the porosity gradient: exponential regression ($R^2 = 0.93$).

Figure 5: Dispersion curves of Lamb modes propagating in a transversely isotropic plate, for three age ranges: [30-39] straight line, [60-69] dots and [80-99] dotted line.

Figure 6: Dispersion curves of the eight first longitudinal modes (in black) and the ten first flexural (in grey) modes propagating in a transversely isotropic tube, for three age ranges: [30-39] straight line, [60-69] dots and [80-99] dotted line.

Figure 7: Group velocity of A_0 mode (in black) and $F(1,1)$ mode (in grey) propagating in a transversely isotropic plate and tube respectively, for

three age ranges: [30-39] straight line, [60-69] dots and [80-99] dotted line.

Tables

Table 1: Elastic properties of cortical bone at the periosteal boundary (per.) and at the endosteal boundary (end.).

		c_{11} (GPa)	c_{12} (GPa)	c_{13} (GPa)	c_{33} (GPa)	c_{44} (GPa)	c_{66} (GPa)	ρ (g/cm^3)
[10-19]	per.	26.33	10.73	11.25	34.17	8.30	7.80	1.88
	end.	25.05	10.22	10.80	32.72	7.83	7.41	1.84
[20-29]	per.	26.30	10.72	11.23	34.13	8.29	7.79	1.88
	end.	24.61	10.05	10.64	32.22	7.67	7.28	1.83
[30-39]	per.	26.10	10.64	11.16	33.90	8.22	7.73	1.87
	end.	24.40	9.97	10.57	31.99	7.60	7.22	1.83
[40-49]	per.	25.08	10.23	10.81	32.76	7.84	7.42	1.85
	end.	22.91	9.38	10.06	30.32	7.05	6.76	1.79
[50-59]	per.	25.08	10.23	10.81	32.76	7.84	7.42	1.85
	end.	22.06	9.04	9.76	29.36	6.74	6.51	1.77
[60-69]	per.	25.69	10.48	11.02	33.44	8.07	7.61	1.86
	end.	22.03	9.03	9.75	29.32	6.73	6.49	1.76
[70-79]	per.	25.05	10.22	10.80	32.72	7.83	7.41	1.84
	end.	20.09	8.27	9.08	27.15	6.02	5.91	1.71
[80-99]	per.	25.15	10.26	10.83	32.83	7.87	7.44	1.85
	end.	18.06	7.47	8.37	24.86	5.28	5.29	1.66

Table 2: Age-related regional evolution in intracortical porosity and gradient.

	t (mm)	p% per. (%)	p% mid. (%)	p% end. (%)	*grad* (%/mm)
[10-19]	3.804	2.4	3.7	6.2	0.999
[20-29]	4.166	2.5	3.75	7.5	1.200
[30-39]	4.368	3.1	4.4	8.1	1.145
[40-49]	4.354	6.1	7.4	12.5	1.470
[50-59]	3.762	6.1	8	15	2.366
[60-69]	3.104	4.3	11.5	15.1	3.479
[70-79]	3.46	6.2	11.3	20.8	4.220
[80-99]	2.502	5.9	17.5	26.8	8.353

Table 3: Geometry of the waveguides for three age ranges.

	thickness (plate or tube)	tube dimensions		
	t (mm)	a_0 (mm)	a_q (mm)	t/a_q
[30-39]	4.368	7.64	12	0.36
[60-69]	3.104	8.9	12	0.26
[80-99]	2.502	9.5	12	0.21

Table 4: Variations in cut-off frequencies for longitudinal and flexural modes with aging.

	L(0,2)	L(0,3)	F(1,2)	F(1,3)	F(1,4)	F(1,5)
$\Delta f_{30/60}$ (kHz)	4.9	88.3	2.9	4.5	87.2	80.8
$\Delta f_{60/80}$ (kHz)	3.4	60.3	2.2	4	60.1	59.7
$\Delta f_{30/80}$ (kHz)	8.3	148.6	5.1	8.4	147.3	140.5

Table 1: Elastic properties of cortical bone at the periosteal boundary (per.) and at the endosteal boundary (end.).

		c_{11} (GPa)	c_{12} (GPa)	c_{13} (GPa)	c_{33} (GPa)	c_{44} (GPa)	c_{66} (GPa)	ρ (g/cm^3)
[10-19]	per.	26.33	10.73	11.25	34.17	8.30	7.80	1.88
	end.	25.05	10.22	10.80	32.72	7.83	7.41	1.84
[20-29]	per.	26.30	10.72	11.23	34.13	8.29	7.79	1.88
	end.	24.61	10.05	10.64	32.22	7.67	7.28	1.83
[30-39]	per.	26.10	10.64	11.16	33.90	8.22	7.73	1.87
	end.	24.40	9.97	10.57	31.99	7.60	7.22	1.83
[40-49]	per.	25.08	10.23	10.81	32.76	7.84	7.42	1.85
	end.	22.91	9.38	10.06	30.32	7.05	6.76	1.79
[50-59]	per.	25.08	10.23	10.81	32.76	7.84	7.42	1.85
	end.	22.06	9.04	9.76	29.36	6.74	6.51	1.77
[60-69]	per.	25.69	10.48	11.02	33.44	8.07	7.61	1.86
	end.	22.03	9.03	9.75	29.32	6.73	6.49	1.76
[70-79]	per.	25.05	10.22	10.80	32.72	7.83	7.41	1.84
	end.	20.09	8.27	9.08	27.15	6.02	5.91	1.71
[80-99]	per.	25.15	10.26	10.83	32.83	7.87	7.44	1.85
	end.	18.06	7.47	8.37	24.86	5.28	5.29	1.66

Table 2: Age-related regional evolution in intracortical porosity and gradient.

	t (mm)	p% per. (%)	p% mid. (%)	p% end. (%)	*grad* (%/mm)
[10-19]	3.804	2.4	3.7	6.2	0.999
[20-29]	4.166	2.5	3.75	7.5	1.200
[30-39]	4.368	3.1	4.4	8.1	1.145
[40-49]	4.354	6.1	7.4	12.5	1.470
[50-59]	3.762	6.1	8	15	2.366
[60-69]	3.104	4.3	11.5	15.1	3.479
[70-79]	3.46	6.2	11.3	20.8	4.220
[80-99]	2.502	5.9	17.5	26.8	8.353

Table 3: Geometry of the waveguides for three age ranges.

	thickness (plate or tube)	tube dimensions		
	t (mm)	a_0 (mm)	a_q (mm)	t/a_q
[30-39]	4.368	7.64	12	0.36
[60-69]	3.104	8.9	12	0.26
[80-99]	2.502	9.5	12	0.21

Table 4: Variations in cut-off frequencies for longitudinal and flexural modes with aging.

	L(0,2)	L(0,3)	F(1,2)	F(1,3)	F(1,4)	F(1,5)
$\Delta f_{30/60}$ (kHz)	4.9	88.3	2.9	4.5	87.2	80.8
$\Delta f_{60/80}$ (kHz)	3.4	60.3	2.2	4	60.1	59.7
$\Delta f_{30/80}$ (kHz)	8.3	148.6	5.1	8.4	147.3	140.5

Figure1

Click here to download Figure: Figure1.pdf

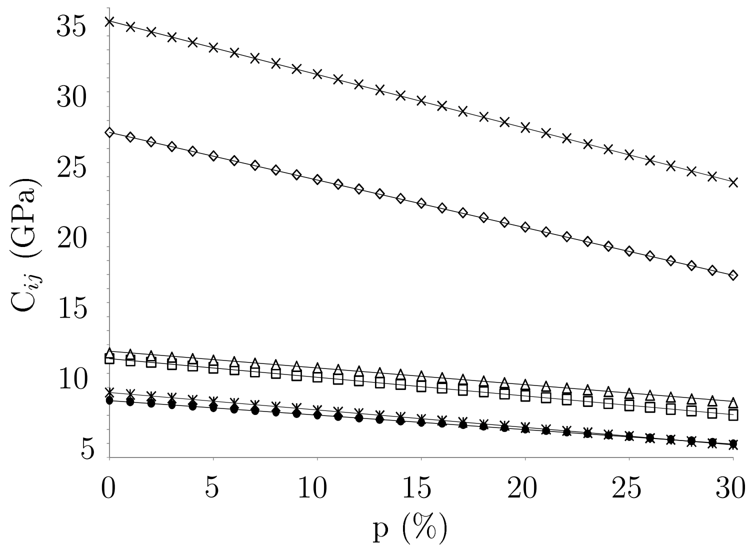

Figure2

Click here to download Figure: Figure2.pdf

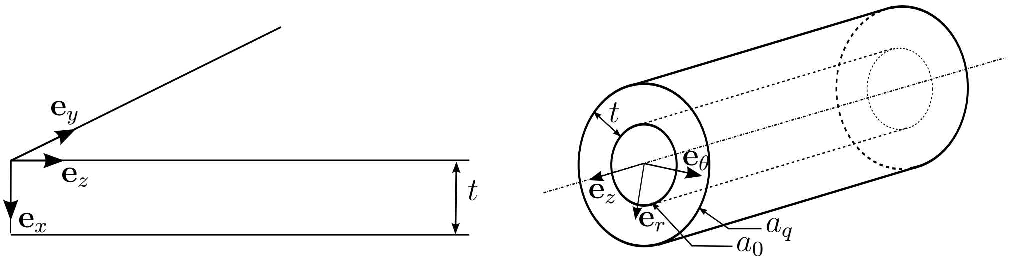

Figure3

Click here to download Figure: Figure3.pdf

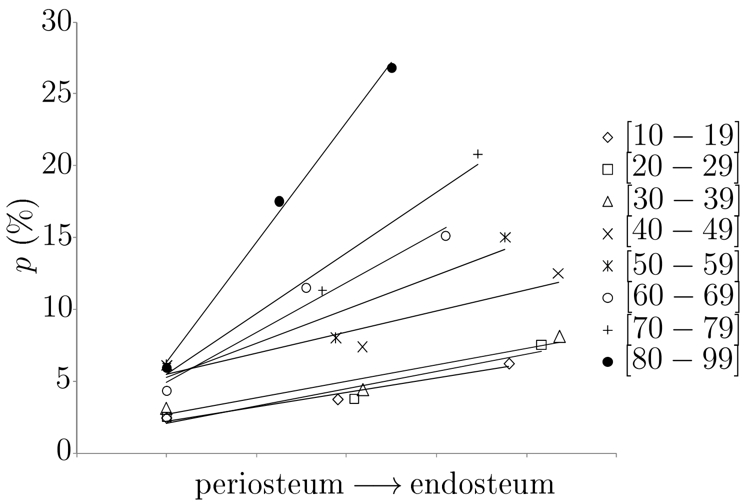

Figure4
Click here to download Figure: Figure4.pdf

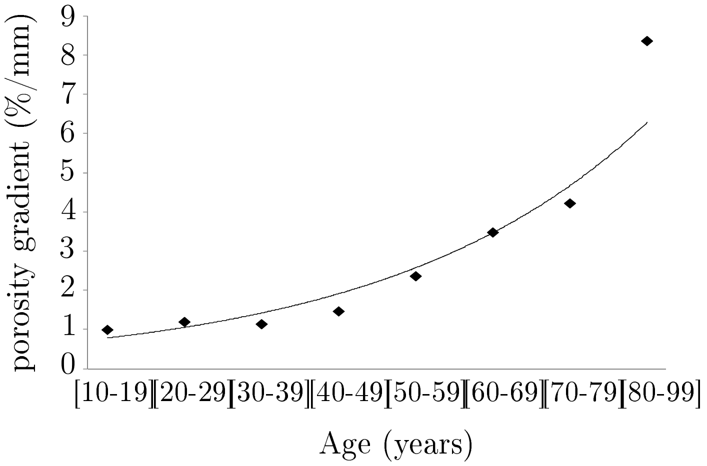

Figure5
[Click here to download Figure: Figure5.pdf]

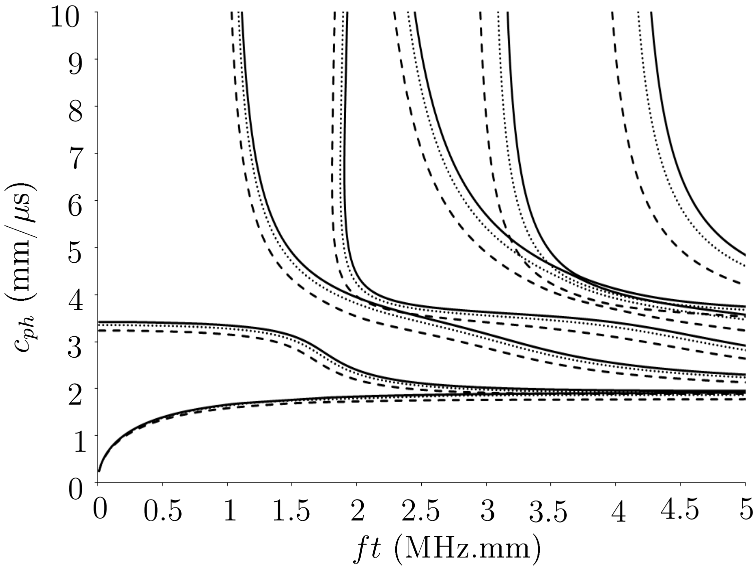

Figure6

Click here to download Figure: Figure6.pdf

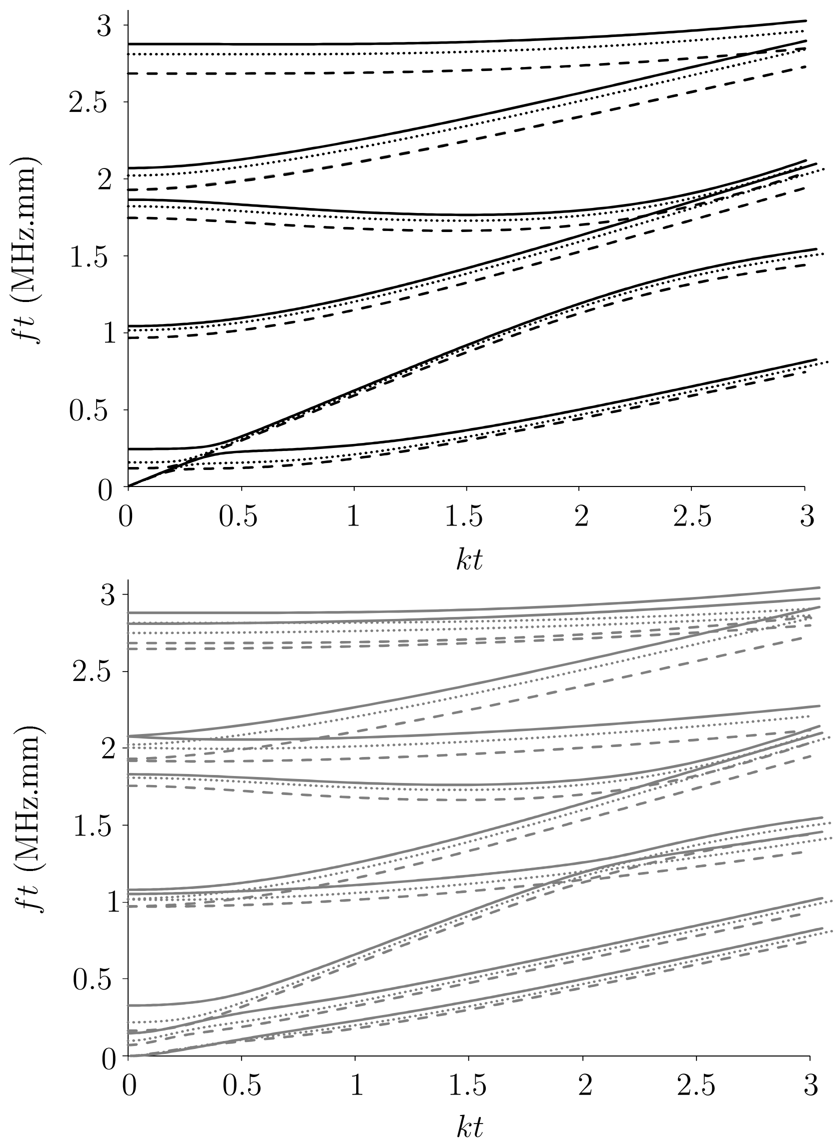

Figure7

Click here to download Figure: Figure7.pdf